Chia-En Wong[1]
Section of Neurosurgery,
Department of Surgery,
National Cheng Kung University Hospital,
College of Medicine,
National Cheng Kung University,
Tainan 704, Taiwan

Hsuan-Teh Hu[1]
Department of Civil Engineering,
National Cheng Kung University,
Tainan 701, Taiwan;
Department of Civil and Disaster Prevention Engineering,
National United University,
Miaoli 360, Taiwan

Cho-Hsuan Tsai
Department of Civil Engineering,
National Cheng Kung University,
Tainan 701, Taiwan

Jun-Liang Li
Department of Otolaryngology,
Tungs' Taichung MetroHarbor Hospital,
Taichung 433, Taiwan

Chin-Chiang Hsieh
Department of Radiology,
Tainan Hospital,
Ministry of Health and Welfare,
Tainan 700, Taiwan

Kuo-Yuan Huang[2]
Department of Orthopedics,
National Cheng Kung University Hospital,
College of Medicine,
National Cheng Kung University,
Tainan 701, Taiwan
e-mail: hkyuan@mail.ncku.edu.tw

Comparison of Posterior Fixation Strategies for Thoracolumbar Burst Fracture: A Finite Element Study

The management of thoracolumbar (TL) burst fractures remained challenging. Due to the complex nature of the fractured vertebrae and the lack of clinical and biomechanical evidence, currently, there was still no guideline to select the optimal posterior fixation strategy for TL burst fracture. We utilized a T10-L3 TL finite element model to simulate L1 burst fracture and four surgical constructs with one- or two-level suprajacent and infrajacent instrumentation (U1L1, U1L2, U2L1, and U2L2). This study was aimed to compare the biomechanical properties and find an optimal fixation strategy for TL burst fracture in order to minimize motion in the fractured level without exerting significant burden in the construct. Our result showed that two-level infrajacent fixation (U1L2 and U2L2) resulted in greater global motion reduction ranging from 66.0 to 87.3% compared to 32.0 to 47.3% in one-level infrajacent fixation (U1L1 and U2L1). Flexion produced the largest pathological motion in the fractured level but the differences between the constructs were small, all within 0.26 deg. Comparisons in implant stress showed that U2L1 and U2L2 had an average 25.3 and 24.8% less von Mises stress in the pedicle screws compared to U1L1 and U1L2, respectively. The construct of U2L1 had better preservation of the physiological spinal motion while providing sufficient range of motion reduction at the fractured level. We suggested that U2L1 is a good alternative to the standard long-segment fixation with better preservation of physiological motion and without an increased risk of implant failure. [DOI: 10.1115/1.4050537]

Keywords: thoracolumbar, burst fracture, posterior fixation, pedicle screw and rod construct, finite element

Introduction

Burst fractures most commonly involved the thoracolumbar (TL) spine [1,2]. Axial compressive momentum on the slightly flexed spine resulted in compression of the anterior column, fracture of the middle column, and potential retropulsion of bone fragments into the spinal canal [3–5]. Spinal instability had been a major concern following traumatic spinal injury. Previously, Denis introduced the concept of the three-column model, and the failure of two columns was considered as an absolute criterion for spinal instability [4]. Since TL burst fractures involved in the failure of both the anterior and the middle column, any TL burst fracture could be considered as unstable [6].

The management of TL burst fractures remained challenging. Alpantiki et al. suggested that nonoperative treatment was appropriate for patients without neurological deficits and with intact posterior ligamentous complex, but delayed neurological deterioration was reported in up to 17% of patients, who often require surgical intervention [1,7–10]. Surgical management of TL burst fractures was aimed to decompress the neural tissue, stabilize the vertebral columns, and prevent further kyphotic deformity, which often requires rigid fixation of the spine segments [2].

Posterior instrumentation (PI) with pedicle screws and rods had been the most widely accepted method for surgical stabilization since it involved rigid fixation of all three columns of the spine [1,11]. Previous results had demonstrated both clinical and radiographic improvement in patients with TL burst fracture after posterior fixation with screw and rod-based constructs [12,13]. Some previous studies addressed the biomechanical characteristics of the fractured TL spine after PI. McLain et al. and Sapkas et al. discussed the biomechanics and the number of instrumented segments in TL burst fractures, and long-segment fixation was associated with better radiographic results [14,15]. Basaran et al. compared short-segment fixation to long-segment fixation and concluded that short-segment fixation was sufficient to create robust stabilization [15]. However, these studies only addressed two constructs, and other designs such as those with a different number of instrumented levels at the suprajacent and infrajacent segments had not been evaluated. As a result, due to the complex nature of the fractured vertebral body and lack of clinical or biomechanical evidence, currently, there was no guideline or standard to select the best posterior fixation strategy for TL burst fracture.

In this study, we established a finite element (FE) model of T10-L3 TL segments and simulated L1 burst fracture. Four

[1]Chia-En Wong and Hsuan-Teh Hu contributed equally to this study.
[2]Corresponding author.
Manuscript received January 2, 2020; final manuscript received March 1, 2021; published online April 7, 2021. Assoc. Editor: Christian Puttlitz.

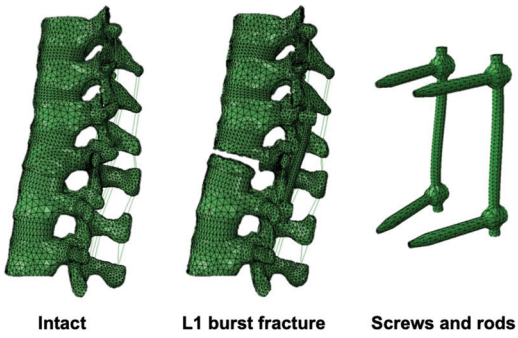

Fig. 1 Finite element model of T10-L3 thoracolumbar spine and simulation of L1 burst fracture with posterior fixation. The present finite element model of the intact spine (left), simulated L1 bust fracture (middle), and the pedicle screws and rods (right).

fixation constructs involving either one- or two-level suprajacent and infrajacent pedicle screw and rod fixation were simulated. Flexion, extension, lateral bending, and axial rotation range of motion (ROM) of both the constructs and the fractured levels were analyzed. The burden of each construct including maximum von Mises stress and strain energy was also compared. The objective of this study was aimed to find an optimal posterior fixation strategy for TL burst fracture in order to minimize motion in the fractured level without creating a significant burden in the construct itself.

Material and Method

Generation of Thoracolumbar Finite Element Model. A three-dimensional FE model of the T10-L3 TL spine segments was created from axial computed tomography images at 1-mm thickness intervals obtained from a resin spine model, which was cast from the cadaveric spine of an Asian male in his thirties without spinal disease or abnormalities. The images were imported into the software 3D-DOCTOR software (Able Software Corp., Lexington, MA) to construct the geometric structure of T10-L3. The mesh structure was prepared using the preprocessing software PATRAN (MSC software, Irvine, CA) and the FE model was imported into ABAQUS 6.12 (Simulia Inc., Johnston, RI) to solve (Fig. 1). For vertebral bone, a closed surface was first generated consisting of cortical bones and endplates assigned to 3-node shell elements (S3R). The thickness of the cortical bones and endplates was set to 0.35 mm and 0.5 mm according to previous studies [16–18]. Inside the cortical surface contained cancellous bone assigned to 4-node solid continuum elements (C3D4).

The intervertebral discs (IVDs) were generated with its superior and inferior boundary being the endplates of the adjacent segmented vertebra. The outer boundary of the IVD was generated according to the scanned geometry. The boundary between the annulus fibrosus and nucleus pulposus was generated parallel to the outer border and making the volume of the nucleus pulposus being 50% of the total IVD volume [19]. The IVDs were modeled with three different components: annulus fibers, annulus ground substance, and nucleus pulposus [20,21]. The annulus was constructed as a ring-shaped structure defined by an outer annulus fiber as the outer border and an inner annulus fiber as the inner border. The annulus fibers were modeled with six layers of shell elements with a thickness of 1.5 mm. Annulus ground substance was modeled by solid tetrahedral elements (C3D4) between the inner and outer layers of annulus fibers. The nucleus pulposus was modeled by noncompressible solid tetrahedral linear elements (C3D4) inside the inner annulus fiber.

The facet was modeled as part of the posterior bony elements according to the original geometry using C3D4 tetrahedron elements as previously described [22]. A three-dimensional surface-to-surface contact with friction was assigned to simulate the facet contact behavior with a finite sliding interaction defined to allow random motions including sliding, rotation, and separation. The friction characteristic was modeled with a classic isotropic Coulomb friction model with friction coefficient of 0.1.

The ligamentous complex including anterior longitudinal ligaments (ALL), posterior longitudinal ligaments (PLL), ligamentum flavum (LF), interspinous ligaments (ISL), and supraspinous ligaments (SSL) was modeled using Truss elements (T3D2). The material properties of the FE models were given in Table 1.

Simulation of Thoracolumbar Burst Fracture. Burst fractures of the TL spine resulted in the failure of the anterior and middle columns under axial loads in the three-column theory [3,4]. In this study, the fractured model was created by removing the elements of the middle 30% of the L1 vertebral body, according to previously described method with some modifications [23]. The ALL and PLL at L1 level were also removed. The fractured model simulated A3-type vertebral burst fracture in the Arbeitsgemeinschaft für Osteosynthesefragen fracture classification [24] (Fig. 1).

Generation of Pedicle Screw and Rod Model for Posterior Fixation. The primary dimensions (diameter, length) of the pedicle screws for thoracic lumbar vertebra were 5.5 mm × 45 mm and 6.5 mm × 45 mm, respectively. The diameter of the rods was 6 mm. The pedicle screws and rods were composed of titanium. The material properties of the implants were shown in Table 1. Three-dimensional structures of the screws and rods were created in software PATRAN (MSC software) (Fig. 1). The mesh structures were prepared using software HYPERMESH 11.0 (Altair Technologies Inc) and imported into ABAQUS 6.12 (Simulia Inc) to solve.

Table 1 Material properties and mesh types of the thoracolumbar finite element model

Component	Young's modulus (MPa)	Poisson's ratio	Element type
Annulus fiber			Shell (STRI3)
Inner laminate : inner layer	360	0.30	
Inner laminate : middle layer	385	0.30	
Inner laminate : outer layer	420	0.30	
Outer laminate : inner layer	440	0.30	
Outer Laminate : Mid-dle Layer	495	0.30	
Outer Laminate : Outer Layer	550	0.30	
Annulus ground substance	4.2	0.45	Tetrahedron (C3D4)
Cancellous bone	100	0.20	Tetrahedron (C3D4)
Cortical bone	12,000	0.30	Shell (S3R)
Posterior bony elements	3500	0.25	Tetrahedron (C3D4)
Endplate	12,000	0.30	Shell (S3R)
Nucleus pulposus	1	0.49	Tetrahedron (C3D4)
ALL/PLL/LF/ISL/SSL	20/20/20/10/10	0.25	Truss (T3D2)
Titanium screw/rod	110,000	0.30	Tetrahedron (C3D4)

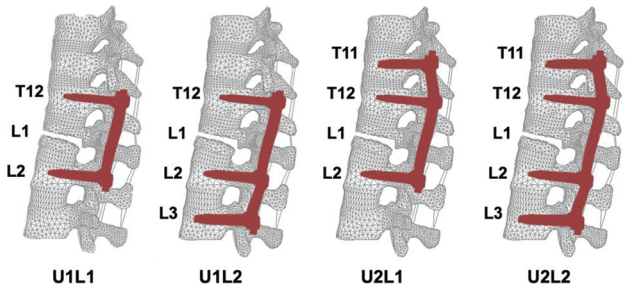

Fig. 2 Different pedicle screw and rod-based constructs. Four fixation constructs for L1 burst fracture simulated in this study including short-segment instrumentation(U1L1), long-segment instrumentation(U2L2), and intermediate constructs (U1L2 and U2L1). The screw and rod constructs are shown in red.

Simulation of Posterior Fixation Surgeries. Five models were simulated in this study. These included an unfractured intact model and four different surgical constructs consisting of bilateral pedicle screw and rod fixation in either one-level or two-level adjacent levels: (1) one-level fixations superior (T12) and inferior (L2) to the fracture level (U1L1); (2) one-level fixation superior (T12) and two-level fixation inferior (L2,L3) to the fracture level (U1L2); (3) two-level fixation superior (T11,T12) and one-level fixation inferior (L2) to the fracture level (U2L1); (4) two-level fixations superior (T11,T12) and inferior (L2,L3) to the fracture level (U2L2) (Fig. 2).

Loading and Boundary Conditions. The preload was set to 150 N and applied evenly using the follower load technique on the superior endplate of the T10 vertebral body to simulate the weight of the upper body. For the simulation of the upper body weight, a preload ranging from 100 to 200 N was used in the literature, and a 150 N preload was chosen in this study [25,26]. The 6 N-m moment was applied in the sagittal, coronal, and transverse plane to create flexion–extension, lateral bending, and axial rotation, respectively.

The boundary condition of the simulations was set with the nodes on the inferior endplate of L3 constrained in all directions. The interfaces of the pedicle screws and bone were assigned with tie constraints.

Result

Model Validation. To validate the present FE model, we compared the ROM of both the intact spine model and the posterior instrumented fractured spine model with the literature (presented as mean and standard deviations). First, the motion of the intact model in T12-L2 was compared to the results of in vitro cadaveric studies by Hitchon et al. and Moon et al. (Fig. 3(*a*)) [27,28]. The comparisons showed the ROM of the present intact model in flexion, extension, and axial rotation was within one standard deviation (SD) when compared to the literature. The ROM in lateral bending was within one SD of that reported by Moon et al. but was smaller (1.19 SD) than one SD compared to the results of Hitchon et al.

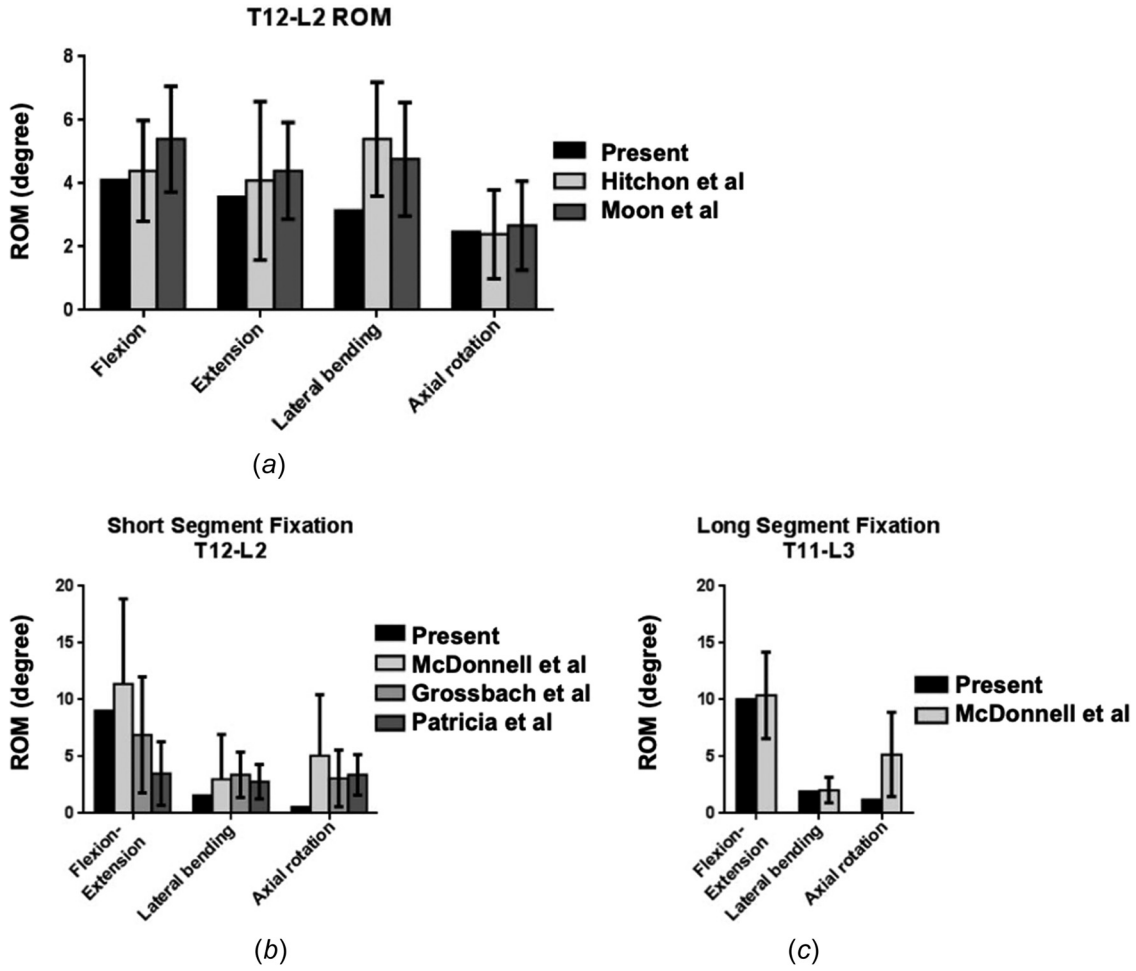

Fig. 3 Validation of the present FE model. Comparisons of the ROM of the present intact (*a*), short-segment fixation (*b*), and long-segment fixation (*c*) models with the literature (presented as mean and standard deviation).

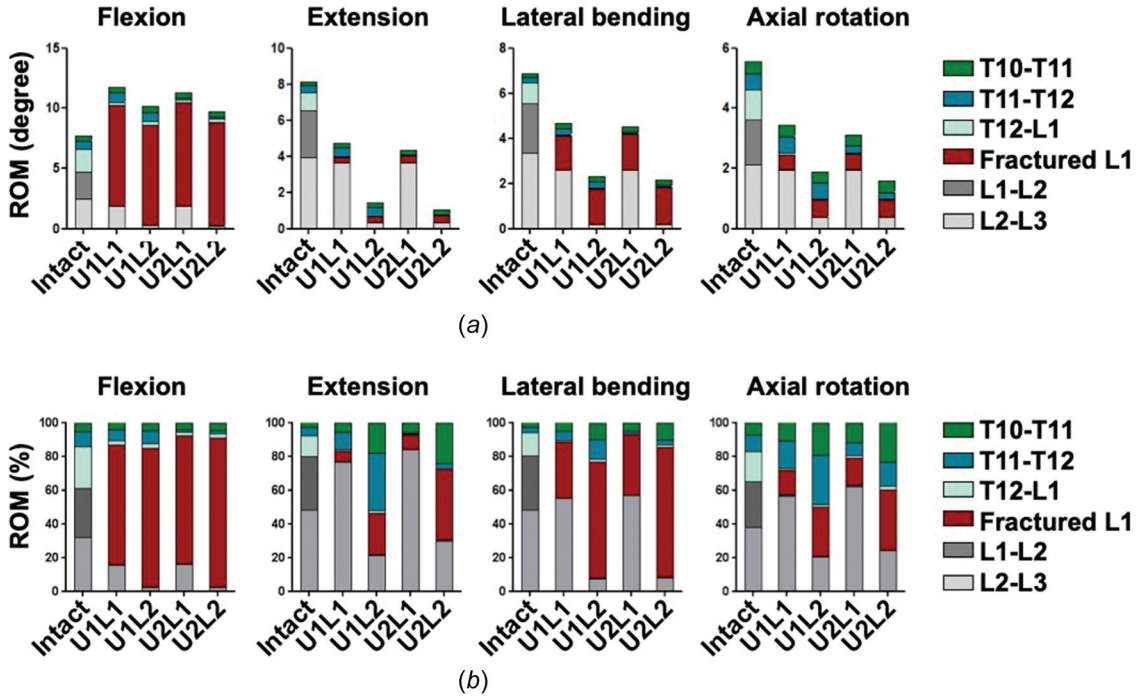

Fig. 4 The range of motion and the ROM distribution in different constructs. The global ROM and ROM distribution presented in absolute value (*a*) and the ROM distribution presented in percentage (*b*).

Next, the fractured and instrumented model was validated against the in vitro cadaveric experiments conducted by McDonnell et al., Grossbach et al., and Patricia et al. [29–31]. For the simulation of short-segment instrumentation, our results were within one SD when compared to the previously reported results except that the ROM in flexion–extension was larger (1.81 SD) than one SD compared to that reported by Patricia et al. and the ROM in rotation was smaller (1.37 SD) than one SD compared to the result of Patricia et al. (Fig. 3(*b*)). For the simulation of long-segment instrumentation, the comparison showed that the ROM of the present model was within one SD when compared to the literature (Fig. 3(*c*)). A detailed discussion about the differences was made in the Discussion section.

Range of Motion and Range of Motion Distribution in the Thoracolumbar Spine. The global flexion, extension, lateral bending, and axial rotation ROM and the ROM distribution of the intact and surgical models were shown in Fig. 4(*a*). Compared to the intact model, all surgeries showed decreased ROM in extension, lateral bending, and axial rotation. However, the ROM in flexion was increased by 53.2, 32.2, 47.4, and 26.5% in U1L1, U1L2, U2L1, and U2L2, respectively. The percentage ROM distributions of the T10-L3 segments in Fig. 4(*b*) further revealed that the increase of motion in flexion was mainly due to the pathological intravertebral motion of L1 caused by the fracture, which accounted for 71.1, 82.3, 76.0, and 88.5% of the global motion in U1L1, U1L2, U2L1, and U2L2, respectively. The comparisons between different fixation constructs showed that more ROM decrease in extension, lateral bending, and rotation was observed in constructs with two-level infrajacent fixation (U1L2 and U2L2), ranging from 66.0 to 87.3% compared to 32.0 to 47.3% in constructs with one-level infrajacent fixation (U1L1 and U2L1).

The Fractured Vertebrae. Burst fractures were considered as unstable fractures, and micromotions or even pseudo-arthrosis could exist at the fracture site, causing mechanical back pain and

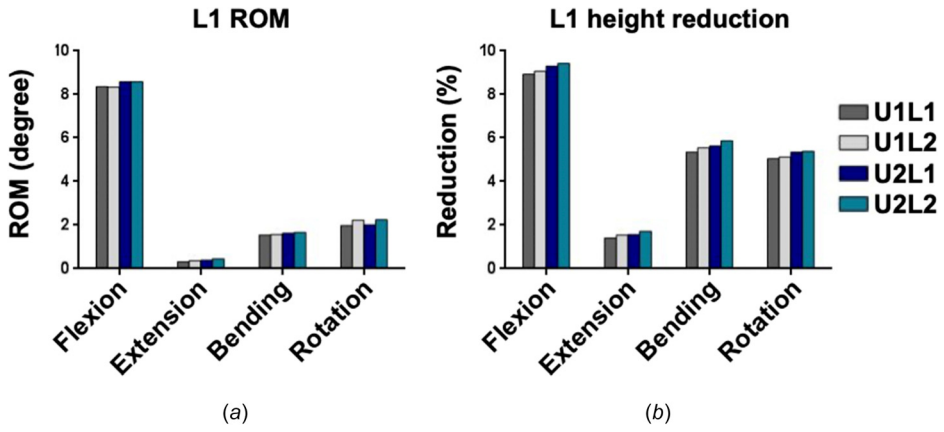

Fig. 5 The fracture motion and the percentage of height reduction in L1. The pathological motion (*a*) and vertebral height reduction (*b*) of the fractured L1 in flexion, extension, lateral bending, and axial rotation.

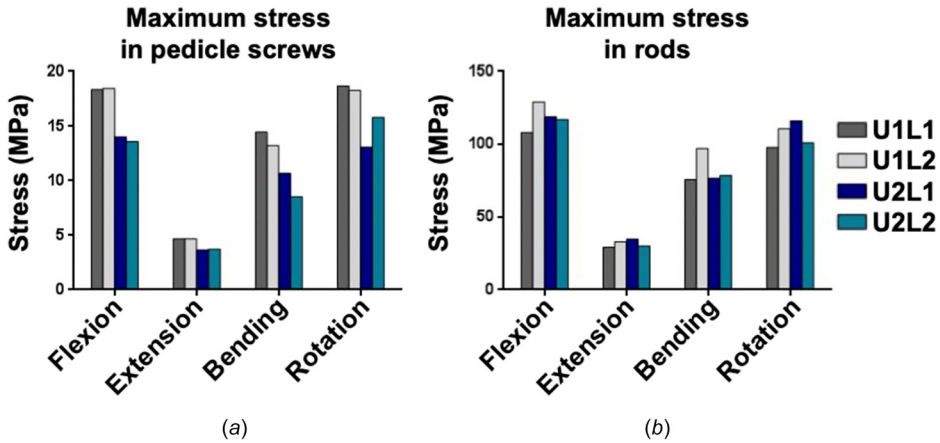

Fig. 6 Maximum von Mises stress in the pedicle screws and the rods in different constructs. The maximum von Mises stress in the pedicle screws (*a*) and the rods (*b*) in flexion, extension, lateral bending, and axial rotation.

neurological complications [11]. The pathological intravertebral ROM within the fractured L1 was shown in Fig. 5(*a*). Flexion produced the largest pathological motion of 8.36, 8.34, 8.60, and 8.59 deg in U1L1, U1L2, U2L1, and U2L2, respectively. The average L1 ROM of the constructs in extension, lateral bending, and axial rotation were 8.4, 0.4, 1.6, and 2.1 deg, respectively. The differences of L1 ROM between the four constructs were small, all within 0.26 deg.

The vertebral height was measured as the distance between the centermost nodes in the superior and inferior endplates of the FE models. Decreased L1 vertebral heights were observed in all fixation constructs (Fig. 5(*b*)). The decrease was dynamic and varied under different spinal motions. Flexion resulted in maximum vertebral height reduction with an average 9.2% decrease of L1 vertebral heights while minimal height reduction was observed in extension with an average 1.5% decrease. An average of 5.6 and 5.2% decrease of L1 vertebral heights was shown in lateral bending and axial rotation, respectively.

The comparison between different constructs showed more height reduction in constructs involving two-level suprajacent fixation to the fractured level. U2L1 resulted in a 9.4, 1.3, 5.2, and 5.4% height reduction and U2L2 resulted in a 9.5, 1.5, 5.4, and 5.4% height reduction whereas U1L1 resulted in a 9.0, 1.2, 4.9, and 5.0% height reduction and U1L2 resulted in a 9.1, 1.3, 5.1, and 5.1% height reduction in flexion, extension, lateral bending, and axial rotation, respectively. Comparisons of changes in L1 vertebral heights between different constructs under different motions revealed the differences were less than 0.6% of the original height.

Von Mises Stress and Strain Energy on the Screw and Rod Construct. The maximum von Mises stress and strain energy of each construct in the pedicle screws and rods under TL motions were shown (Fig. 6). Flexion and axial rotation exerted more mechanical stress on both the screws and rods ranging from 13.6 to 18.7 MPa and 97.9 to 129.4 MPa, respectively. Extension resulted in the least stress for all constructs, with 3.7–4.7 MPa on the screws and 29.3–34.9 MPa on the rods. Comparisons between the constructs showed that U2L1 and U2L2 had an average 25.3 and 24.8% less von Mises stress in the pedicle screws compared to U1L1 and U1L2, respectively. For the rods, U1L2 generated 8.6% and 23.4% more von Mises stress under flexion and lateral bending compared to the second highest value, respectively. U1L2 and U2L1 had 9.6% and 14.9% more stress on the rods under axial rotation compared to the third highest value. The maximum stress at the pedicle screws and rods for each construct and the corresponding motion was given in Table 2.

For all four constructs, the maximum von Mises stresses in the pedicle screws were measured at the base of the T12 pedicle screws near the junction of the screws and rods. For the rods, the maximum von Mises stresses were measured at the L1 level in all

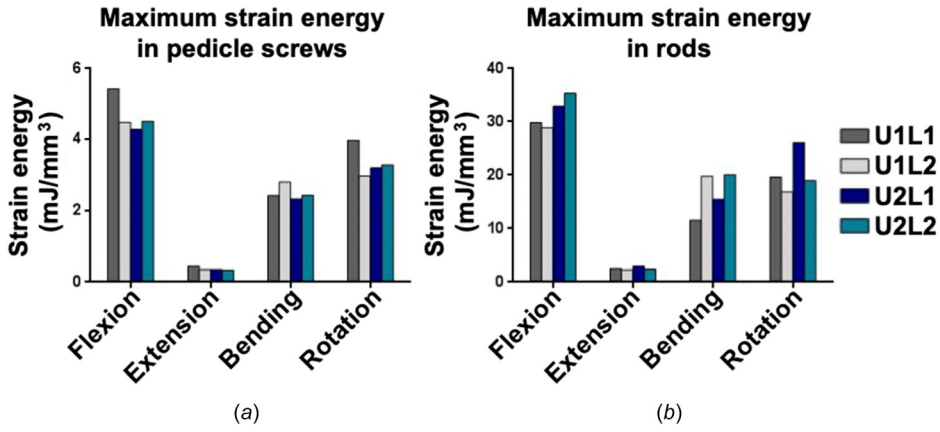

Fig. 7 Maximum strain energy in the pedicle screws and the rods in different constructs. The maximum strain energy in the pedicle screws (*a*) and the rods (*b*) in flexion, extension, lateral bending, and axial rotation.

Table 2 Maximum von Mises stress in the pedicle screws and rods

Maximum stress in the pedicle screws				
Construct	U1L1	U1L2	U2L1	U2L2
Stress (MPa)	18.70	18.49	14.02	15.83
Level	T12	T12	T12	T12
Motion	rotation	flexion	flexion	rotation
Maximum stress in the rods				
Construct	U1L1	U1L2	U2L1	U2L2
Stress (MPa)	108.35	129.36	119.09	117.32
Motion	flexion	flexion	flexion	flexion

Table 3 Maximum strain energy in the pedicle screws and rods

Maximum strain energy in the pedicle screws				
Construct	U1L1	U1L2	U2L1	U2L2
Energy (mJ/mm^3)	5.43	4.48	4.28	4.51
Motion	Flexion	Flexion	Flexion	Flexion
Maximum strain energy in the rods				
Construct	U1L1	U1L2	U2L1	U2L2
Energy (mJ/mm^3)	29.83	28.89	32.90	35.36
Motion	Flexion	Flexion	Flexion	Flexion

constructs. The locations where the maximum stresses in the pedicle screws were measured were presented in Fig. 1 available in the Supplemental Materials on the ASME Digital Collection.

The strain energy in the pedicle screws and rods was presented in Fig. 7. While the difference of pedicle screw strain energy between U1L2, U2L1, and U2L2 was within 13.5%, U1L1 had 20.4% and 21.0% increased strain energy in the pedicle screws compared to the second highest value in flexion and rotation, respectively. The strain energy in the rods was higher under flexion compared to other motion in all constructs. U1L2 and U2L2 had 28.% and 29.9% increased more strain energy under lateral bending compared to U2L1. U2L1 had a 33.0% more strain energy under rotation compared to the second highest value in U1L1. The maximum strain energy at the pedicle screws and the rods for each construct and the corresponding motion was given in Table 3.

Discussion

Posterior instrumentation with pedicle screws and rods had been the most widely accepted approach for surgical stabilization of TL burst fractures [11,12]. Although some previous studies had addressed the biomechanical properties of pedicle screw-based posterior fixation constructs, there was no guideline or standard to select the posterior fixation strategy, and the ideal management remained controversial [32–34]. This study evaluated and compared the biomechanics of different fixation strategies using FE analysis.

The FE model of the TL spine in this study was validated against previously published in vitro data including the ROM of the intact and the instrumented model. The majority of our results remained compatible and within one SD compared to the literature. Although some differences were noted between our results and previous experiments, the differences were within 1.19 SD in the intact model and within 1.81 SD in the instrumented model. It should be noted that the experimental data cited from the literature had high variability, especially in the ROM of the instrumented spine. The variation of the anatomy in the present model and the cadaveric experiments in the literature could result in different response in spinal motion. For the instrumented model, multiple real-world factors in the placement of the pedicle screws including anatomical variation and surgeon's preference could all contribute to the variation in the cadaveric experiments. Moreover, the difference in loading application and the assumption of isotropic materials properties in the FE model might also contribute to the differences since the spinal responses to moments in different planes may be different.

To prevent hypermobility and pseudo-arthrosis, we aimed to optimize posterior fixation in order to minimize the motion in the fractured level without creating a significant burden in the construct itself. The relation between motion at fracture site and hypertrophic pseudo-arthrosis had been well established and that TL region was susceptible to failure of fusion because of its transitional biomechanics [35]. Since T12-L2 was often the site of early micromotion, adequate fixation and stabilization are required to promote fusion and to avoid pseudarthrosis [35,36]. Our simulation showed that all construct had similar ROM at the fractured level under all motions with the difference within 0.26 deg. Comparisons of changes in L1 vertebral heights between different constructs under different motions revealed the differences were less than 0.6% of the original height. With this in mind, the result further suggested that the extent of fixation might not have a significant impact on the fusion of the fractured level.

In terms of global ROM, our result showed that U1L1 and U2L1 had better physiological ROM preservation with only 32.0 to 47.3% ROM reduction compared to 66.0–87.3% ROM reduction observed in U1L2 and U2L2 during extension, lateral bending, and rotation. For ROM distribution, U1L1 and U2L1 had less ROM percentage in the fractured L1 level.

This study investigated the maximum von Mises stress and strain energy in the implants rather than in the vertebral bone because of the effect of stress shielding after PI, which was previously described [37]. Previous results showed that in the cases of instrumented lumbar fusion, PI shifted the axial load posteriorly with more than 50% of compressive load shifted to the pedicle screws and rods [38]. The percentage would be higher in the present scenario since TL burst fractures resulted in complete failure of the anterior and middle column [6]. As a result, the axial load would mostly be exerted on the construct and risk of early implant failure would be higher. We aimed to investigate the construct burden to minimize the risks of implant failure. Regarding the von Mises stress and strain energy in the pedicle screws and rods, the maximum von Mises stress of the constructs was related to the risks of acute implant fracture since material failure occurs when the von Mises stress surpasses the tensile yield stress [39]. However, acute failure of the screws and rods would be less likely unless there was any major trauma since the tensile yield stress of titanium is approximately 880 MPa and the maximum stress in the present simulation is 129.4 MPa in the rods of U1L1 under flexion.

Material fatigue was related to cyclic strain energy during repetitive motion, and therefore the strain energy in the constructs could be interpreted as the susceptibility to implant failure due to chronic wearing [40]. As a result, the strain energy might be a better parameter to evaluate the susceptibility of the titanium screws and rods to implant failure. Our comparison showed that higher strain energy in both the pedicle screws and the rods was observed flexion compared to other motion in all constructs. Regarding the pedicle screws, U1L1 had more strain energy under flexion and rotation compared to other constructs. On the other hand, the strain energy in the rods was different in each construct under different motion. Since previous studies concluded that the most common implant failure was pedicle screw failure, our result suggested that short segment fixation U1L1 might be at higher risks of implant failure [41,42].

Taken together, our results suggested that the construct of U2L1 had better preservation of the physiological spinal motion and provided sufficient ROM reduction at the fractured level. Although short segment fixation could sufficiently provide similar ROM reduction and fixation, U1L1 might be at higher risks of implant failure.

The limitations of this study should be noted. First, the complex nature of different fracture morphologies in TL burst fractures and

their impacts on the spinal biomechanics were simplified. Differences in the fracture morphology were likely to alter the ROM and stress distribution but this was very challenging to be taken into account since there are no identical fractures in the real world. Additionally, serving as the transitional area between the rigid thoracic spine and mobile lumbar spine, the TL junction featured unique biomechanics. As a result, changing the level of the fracture and levels of posterior fixation were also likely to alter the biomechanical response of the TL segments. With this in mind, we selected the level with the highest incidence of burst fracture for simulation [43]. Second, simplification of the material properties including the assumption of linear isotropic materials in the FE model might not reflect the real-world behavior of the tissues and the surgical constructs. Third, the contact between the bone and the pedicle screws was set to tie constraints and assumed to be perfect. However, the main conclusions of this study were based on comparisons between the surgical construct models. The above-mentioned model simplifications were equally applied to all models and likely had a minimal effect on the comparative differences.

In conclusion, we utilized a FE model to compare the biomechanical performances of different posterior fixation strategies for TL burst fracture. Our results suggested that two-level suprajacent and one-level infrajacent pedicle screw and rod fixation was a good alternative to the standard long-segment fixation with better preservation of physiological motion and without an increased risk of implant failure.

Funding Data

- Ministry of Science and Technology of Taiwan (MOST 108-2314-B-006 -048 -MY2; Funder ID: 10.13039/501100004663).

Conflict of Interest

The authors declare no conflicts of interest related to this paper.

References

[1] Alpantaki, K., Bano, A., Pasku, D., Mavrogenis, A. F., Papagelopoulos, P. J., Sapkas, G. S., Korres, D. S., and Katonis, P., 2010, "Thoracolumbar Burst Fractures: A Systematic Review of Management," Orthopedics, **33**(6), pp. 422–429.

[2] Dai, L.-Y., Jiang, S.-D., Wang, X.-Y., and Jiang, L.-S., 2007, "A Review of the Management of Thoracolumbar Burst Fractures," Surg. Neurol., **67**(3), pp. 221–231 (discussion 231).

[3] Tang, P., Long, A., Shi, T., Zhang, L., and Zhang, L., 2016, "Analysis of the Independent Risk Factors of Neurologic Deficit After Thoracolumbar Burst Fracture," J. Orthop. Surg. Res., **11**(1), p. 128.

[4] Denis, F., 1983, "The Three Column Spine and Its Significance in the Classification of Acute Thoracolumbar Spinal Injuries," Spine, **8**(8), pp. 817–831.

[5] Holmes, J. F., Miller, P. Q., Panacek, E. A., Lin, S., Horne, N. S., and Mower, W. R., 2001, "Epidemiology of Thoracolumbar Spine Injury in Blunt Trauma," Acad. Emerg. Med., **8**(9), pp. 866–872.

[6] Petersilge, C. A., and Emery, S. E., 1996, "Thoracolumbar Burst Fracture: Evaluating Stability," Semin. Ultrasound, CT, MR, **17**(2), pp. 105–113.

[7] Rajasekaran, S., 2010, "Thoracolumbar Burst Fractures Without Neurological Deficit: The Role for Conservative Treatment," Eur. Spine J., **19**(Suppl 1), pp. S40–S47.

[8] Denis, F., Armstrong, G. W., Searls, K., and Matta, L., 1984, "Acute Thoracolumbar Burst Fractures in the Absence of Neurologic Deficit. A Comparison Between Operative and Nonoperative Treatment," Clin. Orthop. Relat. Res., **189**, pp. 142–149.

[9] Mumford, J., Weinstein, J. N., Spratt, K. F., and Goel, V. K., 1993, "Thoracolumbar Burst Fractures. The Clinical Efficacy and Outcome of Nonoperative Management," Spine, **18**(8), pp. 955–970.

[10] Khattak, M. J., Syed, S., and Lakdawala, R. H., 2010, "Operative Management of Unstable Thoracolumbar Burst Fractures," J. Coll. Phys. Surg., **20**(5), pp. 347–349.

[11] Wood, K. B., Li, W., Lebl, D. R., Lebl, D. S., and Ploumis, A., 2014, "Management of Thoracolumbar Spine Fractures," Spine J., **14**(1), pp. 145–164.

[12] Been, H. D., and Bouma, G. J., 1999, "Comparison of Two Types of Surgery for Thoraco-Lumbar Burst Fractures: Combined Anterior and Posterior Stabilisation vs. Posterior Instrumentation Only," Acta Neurochir., **141**(4), pp. 349–357.

[13] Defino, H. L. A., and Canto, F. R. T., 2007, "Low Thoracic and Lumbar Burst Fractures: Radiographic and Functional Outcomes," Eur. Spine J., **16**(11), pp. 1934–1943.

[14] McLain, R. F., 2006, "The Biomechanics of Long Versus Short Fixation for Thoracolumbar Spine Fractures," Spine, **31**(11 Suppl), pp. S70–S79 (discussion S104).

[15] Basaran, R., Efendioglu, M., Kaksi, M., Celik, T., Mutlu, İ., and Ucar, M., 2019, "Finite Element Analysis of Short Versus Long Segment Posterior Fixation for Thoracolumbar Burst Fracture," World Neurosurg., **128**, pp. e1109–e1117.

[16] Chen, H., Zhou, X., Fujita, H., Onozuka, M., and Kubo, K. Y., 2013, "Age-Related Changes in Trabecular and Cortical Bone Microstructure," Int. J. Endocrinol., **2013**, pp. 1–9.

[17] Palepu, V., Rayaprolu, S. D., and Nagaraja, S., 2019, "Differences in Trabecular Bone, Cortical Shell, and Endplate Microstructure Across the Lumbar Spine," Int. J. Spine Surg., **13**(4), pp. 361–370.

[18] Zehra, U., Brown, K. R., Adams, M. A., and Dolan, P., 2015, "Porosity and Thickness of the Vertebral Endplate Depend on Local Mechanical Loading," Spine, **40**(15), pp. 1173–1180.

[19] Newell, N., Little, J. P., Christou, A., Adams, M. A., Adam, C. J., and Masouros, S. D., 2017, "Biomechanics of the Human Intervertebral Disc: A Review of Testing Techniques and Results," J. Mech. Behav. Biomed. Mater., **69**, pp. 420–434.

[20] Yoganandan, N., Kumaresan, S., Voo, L., and Pintar, F. A., 1996, "Finite Element Applications in Human Cervical Spine Modeling," Spine, **21**(15), pp. 1824–1834.

[21] Kumaresan, S., Yoganandan, N., and Pintar, F. A., 1999, "Finite Element Analysis of the Cervical Spine: A Material Property Sensitivity Study," Clin. Biomech., **14**(1), pp. 41–53.

[22] Wong, C., Hu, H., Hsieh, M., and Huang, K., 2020, "Optimization of Three-Level Cervical Hybrid Surgery to Prevent Adjacent Segment Disease: A Finite Element Study," Front. Bioeng. Biotechnol., **8**(154), p. 154.

[23] Hsieh, Y. Y., Kuo, Y. J., Chen, C. H., Wu, L. C., Chiang, C. J., and Lin, C. L., 2020, "Biomechanical Assessment of Vertebroplasty Combined With Cement-Augmented Screw Fixation for Lumbar Burst Fractures: A Finite Element Analysis," Appl. Sci., **10**(6), pp. 1–14.

[24] Mirza, S. K., Mirza, A. J., Chapman, J. R., and Anderson, P. A., 2002, "Classifications of Thoracic and Lumbar Fractures: Rationale and Supporting Data," J. Am. Acad. Orthop. Surg., **10**(5), pp. 364–377.

[25] Oda, I., Cunningham, B. W., Lee, G. A., Abumi, K., Kaneda, K., and McAfee, P. C., 2000, "Biomechanical Properties of Anterior Thoracolumbar Multisegmental Fixation: An Analysis of Construct Stiffness and Screw-Rod Strain," Spine, **25**(18), pp. 2303–2311.

[26] Bishop, F. S., Samuelson, M. M., Finn, M. A., Bachus, K. N., Brodke, D. S., and Schmidt, M. H., 2010, "The Biomechanical Contribution of Varying Posterior Constructs Following Anterior Thoracolumbar Corpectomy and Reconstruction," J. Neurosurg. Spine, **13**(2), pp. 234–239.

[27] Hitchon, P. W., Goel, V. K., Rogge, T. N., Torner, J. C., Dooris, A. P., Drake, J. S., Yang, S. J., and Totoribe, K., 2000, "In Vitro Biomechanical Analysis of Three Anterior Thoracolumbar Implants," J. Neurosurg. Spine, **93**(2), pp. 252–258.

[28] Moon, S.-M., Ingalhalikar, A., Highsmith, J. M., and Vaccaro, A. R., 2009, "Biomechanical Rigidity of an All-Polyetheretherketone Anterior Thoracolumbar Spinal Reconstruction Construct: An In Vitro Corpectomy Model," Spine J., **9**(4), pp. 330–335.

[29] McDonnell, M., Shah, K. N., Paller, D. J., Thakur, N. A., Koruprolu, S., Palumbo, M. A., and Daniels, A. H., 2016, "Biomechanical Analysis of Pedicle Screw Fixation for Thoracolumbar Burst Fractures," Orthopedics, **39**(3), pp. e514–e518.

[30] Grossbach, A. J., Viljoen, S. V., Hitchon, P. W., DeVries Watson, N. A., Grosland, N. M., and Torner, J., 2015, "Vertebroplasty Plus Short Segment Pedicle Screw Fixation in a Burst Fracture Model in Cadaveric Spines," J. Clin. Neurosci., **22**(5), pp. 883–888.

[31] Kallemeier, P. M., Beaubien, B. P., Buttermann, G. R., Polga, D. J., and Wood, K. B., 2008, "In Vitro Analysis of Anterior and Posterior Fixation in an Experimental Unstable Burst Fracture Model," J. Spinal Disord. Tech., **21**(3), pp. 216–224.

[32] Modi, H. N., Chung, K. J., Seo, I. W., Yoon, H. S., Hwang, J. H., Kim, H. K., Noh, K. C., and Yoo, J. H., 2009, "Two Levels Above and One Level Below Pedicle Screw Fixation for the Treatment of Unstable Thoracolumbar Fracture With Partial or Intact Neurology," J. Orthop. Surg. Res., **4**(1), p. 28.

[33] Altay, M., Ozkurt, B., Aktekin, C. N., Ozturk, A. M., Dogan, O., and Tabak, A. Y., 2007, "Treatment of Unstable Thoracolumbar Junction Burst Fractures With Short- or Long-Segment Posterior Fixation in Magerl Type a Fractures," Eur. Spine J., **16**(8), pp. 1145–1155.

[34] Aly, T. A., 2017, "Short Segment Versus Long Segment Pedicle Screws Fixation in Management of Thoracolumbar Burst Fractures: Meta-Analysis," Asian Spine J., **11**(1), pp. 150–160.

[35] Reid, J. J., Johnson, J. S., and Wang, J. C., 2011, "Challenges to Bone Formation in Spinal Fusion," J. Biomech., **44**(2), pp. 213–220.

[36] Heggeness, M. H., and Esses, S. I., 1991, "Classification of Pseudarthroses of the Lumbar Spine," Spine, **16**(8 Suppl), pp. S449–S454.

[37] Ponnappan, R. K., Serhan, H., Zarda, B., Patel, R., Albert, T., and Vaccaro, A. R., 2009, "Biomechanical Evaluation and Comparison of

Polyetheretherketone Rod System to Traditional Titanium Rod Fixation," Spine J., **9**(3), pp. 263–267.
[38] Cunningham, B. W., Kotani, Y., McNulty, P. S., Cappuccino, A., and McAfee, P. C., 1997, "The Effect of Spinal Destabilization and Instrumentation on Lumbar Intradiscal Pressure: An In vitro Biomechanical Analysis," Spine, **22**(22), pp. 2655–2663.
[39] Doblaré, M., García, J. M., and Gómez, M. J., 2004, "Modelling Bone Tissue Fracture and Healing: A Review," Eng. Fract. Mech., **71**, pp. 13–14.
[40] Pattin, C. A., Caler, W. E., and Carter, D. R., 1996, "Cyclic Mechanical Property Degradation During Fatigue Loading of Cortical Bone," J. Biomech., **29**(1), pp. 69–79.
[41] Xu, B., Tang, T., and Yang, H., 2009, "Long-Term Results of Thoracolumbar and Lumbar Burst Fractures After Short-Segment Pedicle Instrumentation, With Special Reference to Implant Failure and Correction Loss," Orthop. Surg., **1**(2), pp. 85–93.
[42] McLain, R. F., Sparling, E., and Benson, D. R., 1993, "Early Failure of Short-Segment Pedicle Instrumentation for Thoracolumbar Fractures. A Preliminary Report," J. Bone Jt. surgery. Am., **75**(2), pp. 162–167.
[43] Machino, M., Yukawa, Y., Ito, K., Nakashima, H., and Kato, F., 2011, "Posterior/Anterior Combined Surgery for Thoracolumbar Burst Fractures–Posterior Instrumentation With Pedicle Screws and Laminar Hooks, Anterior Decompression and Strut Grafting," Spinal Cord, **49**(4), pp. 573–579.